ACS Catalysis

Research Article

pubs.acs.org/acscatalysis

# On the Way to Biofuels from Furan: Discriminating Diels–Alder and Ring-Opening Mechanisms

S. Vaitheeswaran,[†,‡] Sara K. Green,[‡] Paul Dauenhauer,[‡] and Scott M. Auerbach*[,†,‡]

[†]Department of Chemistry and [‡]Department of Chemical Engineering, University of Massachusetts, Amherst Massachusetts 01003, United States

Supporting Information

**ABSTRACT:** We performed kinetics experiments and quantum calculations to investigate the reaction of furan to benzofuran catalyzed by the acidic zeolite HZSM-5, which is a key step in the conversion of biomass to biofuels through catalytic fast pyrolysis. The reaction was studied experimentally by placing the zeolite in contact with solution-phase furan and detecting the benzofuran product over the temperature range 270–300 °C, yielding an apparent activation energy of 72 ± 3 kJ/mol. The reaction was modeled in gas and zeolite phases to determine the energetics of the following two competing pathways: a Diels–Alder mechanism often assumed in interpretations of experimental data and a ring-opening pathway predicted by the chemoinformatic software RING. Quantum calculations on the zeolite/guest system were performed using the ONIOM embedded cluster approach. We computed the energetics of reactants, products, and all intermediate steps. Locating relevant transition states fell beyond our computational resources because of system size and the ruggedness of the energy landscape. The Diels–Alder mechanism in the gas phase was found to pass through a high-energy intermediate roughly 380 kJ/mol above the reactant energy, which reduces to approximately 200 kJ/mol in HZSM-5. In contrast, the ring-opening mechanism passes through a gas-phase intermediate roughly 500 kJ/mol above the reactant energy, which falls to approximately 50 kJ/mol in HZSM-5. The energy of the ring-opening mechanism over HZSM-5 fits into the experimentally determined energy "budget" of 72 ± 3 kJ/mol. These experimental and computational results highlight the importance of the ring-opening mechanism for this key step in making biofuels. Our results strongly indicate that, in the cavities of HZSM-5, the condensation of two furan molecules to form benzofuran and water does not proceed by a Diels–Alder reaction between the reactants.

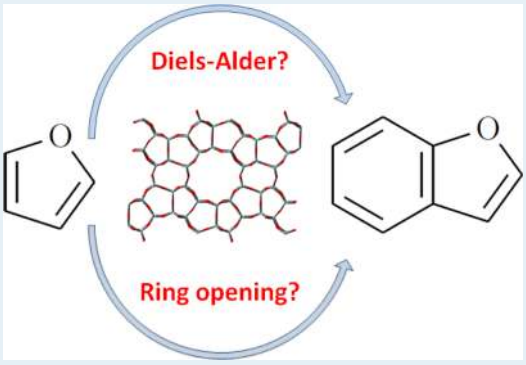


**KEYWORDS:** *biofuels, catalytic pyrolysis, furan, Diels–Alder, HZSM-5, zeolite catalysis, ONIOM, QM/MM*

## 1. INTRODUCTION

Catalytic fast pyrolysis of biomass, involving rapid heating of biomass in the presence of nanoporous zeolite catalysts such as HZSM-5,[1] has proven to be a promising route for converting a variety of biomass sources into aromatic–range biofuels.[2] While this is an attractive approach, only a fraction of the biomass carbon ends up in the resulting fuel (in effect increasing the price of this cellulosic biofuel), largely because of the tendency to form solid carbonaceous materials (i.e., "coke") in the process. Optimization of this technology has been hampered by a lack of fundamental understanding of the catalytic mechanisms at play. Previous experimental studies[3,4] have shown that furan is a good proxy for vapors that arise during cellulose pyrolysis, and that benzofuran is made in HZSM-5 nanopores as an intermediate on the way to making aromatic–range biofuels (Figure 1). However, there is no information on the mechanism by which benzofuran is made, nor is there substantial evidence that the process from furan to benzofuran occurs via Diels–Alder cycloaddition, which has been assumed in the literature.[3] To address this issue, we performed experiments and calculations to obtain fundamental insights into this key step in catalytic fast pyrolysis.

There are a great many possible mechanisms by which two furans may condense to form benzofuran and water. To assist in the identification and enumeration of plausible pathways for complex reactions, chemoinformatic software tools have been created that codify a set of assumed rules of chemistry and chemical mechanisms. One specific example is the Rule Input Network Generator program or RING,[5] which is an automated reaction network generation and analysis tool. Given certain rules and constraints, such as the maximum number of allowed steps, RING generates possible reaction networks connecting given reactants and products. However, these codes do not compute energetics, nor do they account for catalytic surfaces or active sites. As such, we advocate taking plausible outputs from codes like RING as inputs to accurate energy calculation methods such as density functional theory (DFT). One

Received: May 24, 2013
Revised: July 25, 2013
Published: July 26, 2013

   dx.doi.org/10.1021/cs4003904 | ACS Catal. 2013, 3, 2012–2019

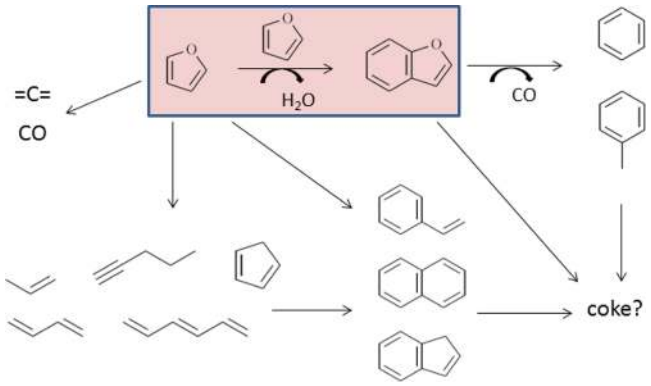


**Figure 1.** Potential chemical reactions during furan pyrolysis at 600 °C. The colored box highlights the key step that is investigated in the present work.

challenge with this translation, which we address below, is that RING outputs bonding patterns using the Lewis−structure language of valence−bond theory, while accurate energies are computed using the molecular−orbital language of DFT. In the work described below, we compute energetics for a ring-opening pathway suggested by RING as a mechanism competing with Diels−Alder cycloaddition for converting furan into benzofuran.

Several computational studies have provided mechanistic information on pathways for processing select biomass-derived species. For example, recent theoretical studies of the conversion of biomass-derived compounds like fructose, glucose, and 5-hydroxymethylfurfural (HMF) have been investigated in the gas phase or in aqueous solution using quantum chemical methods.[6−10] Other researchers have used Car−Parrinello molecular dynamics with metadynamics to study the conversion of glucose in aqueous acids.[11,12] Cluster models of the zeolite HZSM-5 have been used to probe the relatively simple process of protonating fructose.[13] The zeolite-catalyzed cycloaddition of small olefins and substituted furans has also been modeled.[14] However, these particular calculations were performed without a representation of the cage structure of the zeolite catalyst, leaving open the question of shape-selective effects. Explicit inclusion of the zeolite framework in the energy calculations is thus an important step forward in understanding zeolite-catalyzed biomass conversion, which we pursue in the present work by considering sufficiently large embedded cluster models of HZSM-5.

Below we investigate relatively large system sizes with many degrees of freedom, making the search for relevant transition states extremely challenging, especially for rugged energy landscapes. We show below that by combining experimental and computational data, we can still discriminate between Diels−Alder and ring-opening mechanisms without having to compute transition states. In particular, we find that although the Diels−Alder pathway involves lower energies in the gas phase, the ring-opening process is much more favored in the zeolite, with energetics that fit well within the energy budget determined by kinetic experiments.

The remainder of this article is organized as follows: in section 2, we describe the experimental and computational methods pursued below; in section 3, we provide results and discussion on the experiments and on the calculations for both gas-phase and zeolite-catalyzed systems; and in section 4, we offer concluding remarks.

## 2. METHODS

**2.1. Experimental Section.** We measured the activation energy for the formation of benzofuran from furan, catalyzed by HZSM-5. Experiments were conducted in a 100 mL high-pressure, high-temperature batch reactor equipped with a gas entrainment impeller from Parr Instrument Co. (model 4598HTHP). The reaction solution consisted of 60 mL of 1 M furan (Acros Organics, 99%) in heptane (Alfa Aesar, 99%) with 1 mL of *n*-tridecane (Acros Organics, 99%) used as an internal standard. HZSM-5 (CBV−3024E, Zeolyst) with a Si/Al ratio of 15 was calcined at 600 °C in a muffle furnace for at least 6 h and was used with a loading of 0.25 g catalyst to 0.06 mols reactant (i.e., 60 mL of 1 M furan with 0.25 g HZSM-5). The catalyst had a surface area of 405 $m^2\ g^{-1}$, a Brønsted acid site density of 0.71 mmol $g^{-1}$, as measured using isopropylamine TPD-TGA, and a total acid site density of 1.10 mmol $g^{-1}$, as measured using ammonia TPD. Prior to each experiment, the reactor vessel was purged with $N_2$. The reactor vessel was then stirred at a rate of 900 rpm while heating to the desired temperature between 270−300 °C. An initial sample was taken once the desired temperature was achieved and subsequent samples were taken at 10 min intervals for the first 30 min of reaction such that furan conversion was less than 10%. Standard error was calculated for the 90% confidence interval. Liquid samples were analyzed by an Agilent 7890A gas chromatography system, equipped with a Restek Stabilwax−DA capillary column and an FID detector. Helium was used as the carrier gas with a column flow rate of 30 mL/min. One microliter liquid sample was injected for each analysis. Initial rates of benzofuran production were fitted to the Arrhenius temperature dependence to extract an apparent activation energy.

**2.2. Computational Section.** We commenced our theoretical study by applying the cheminformatics program RING.[5] Given a set of

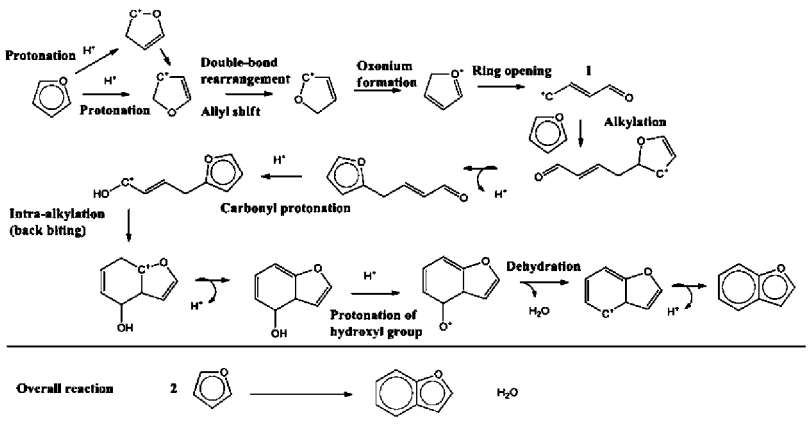


**Figure 2.** Pathway and output produced by RING[5] for the acid catalyzed conversion of furan to benzofuran.


dx.doi.org/10.1021/cs4003904 | ACS Catal. 2013, 3, 2012−2019

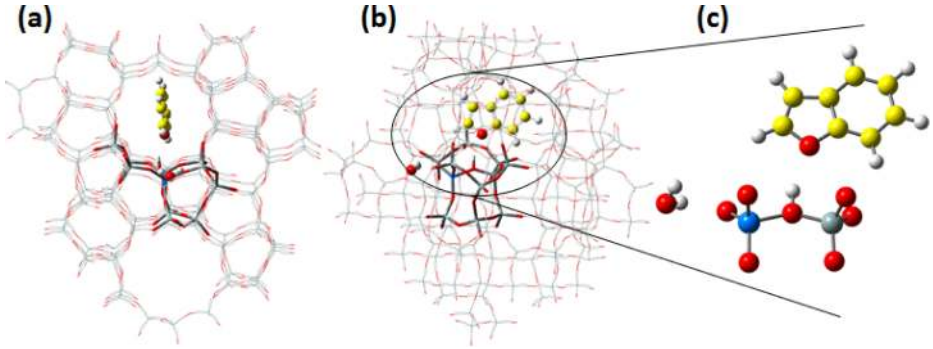


**Figure 3.** Geometry optimized configuration of benzofuran and water in the HZSM-5 cluster, viewed (a) along the straight channel and (b) perpendicular to the straight channel. The quantum mechanical (QM) layer in the zeolite cluster is shown in tube representation, the molecular mechanics (MM) layer in wire frame, and the adsorbates in the ball−and−stick model. Panel c shows the same perspective as panel b, but only the adsorbates and zeolite atoms within two bonds of the acid site are shown, all in ball-and-stick representation. Atom color key: yellow, C; red, O; gray, Si; blue, Al; white, H.

reactants, products, and reaction rules, RING generates a network of reactions that can be used to generate a "first-guess" pathway for the process of interest. In the absence of a comprehensive understanding of the zeolite-catalyzed chemistry of oxygenated compounds like furan, reaction rules have to be based on solution-phase or gas-phase organic chemistry, or experimental observations on related systems. A priori decisions have to be made on which chemical reactions and intermediate species need to be considered by the program and which ones may be disregarded. Hence, the results obtained from RING may be subjective, reflecting the chemical intuition of the user. Nevertheless, it is a very useful tool for identifying the chemical species and elementary reactions that are likely to be important.

For the process of two furans reacting to yield benzofuran and water, we used RING to generate pathways with a (i) list of possible reactions and (ii) the following two constraints: pathways must have no more than 8 steps, and they must be acid-catalyzed. The second constraint was chosen based on experimental observations that the conversion of furan over silicalite (the all-silica analog of HZSM-5) does not lead to the desired aromatic products.[3] The list of possible reactions considered by RING included standard acid catalysis reactions such as protonation/deprotonation, dehydration, oligomerization, ring-opening/closing, and hydrogen transfer reactions.[15] In addition, carbonylation/decarbonylation steps were included[15] to account for Cheng et al.'s experimental detection of carbon monoxide.[3] This yielded the reaction pathway shown in Figure 2.

The pathway in Figure 2 indicates that the acid-catalyzed conversion of furan to benzofuran is initiated by the protonation and ring-opening of a furan molecule, followed by the alkylation of a second furan. Using this pathway as a guide, we exhaustively explored all possible protonated and ring-opened derivatives of furan. In subsequent steps, we explored chemical species as thoroughly as our computational resources allowed. In the zeolite, we sampled 5−10 relevant orientations/conformations of each guest molecule in the HZSM-5 intersection. Conformations that were judged as unlikely to lead to the next step, for example, requiring very long-range proton transfer, were treated as off-pathway "dead ends" and were discarded. The lowest energy conformation of each intermediate was used to construct the zeolite-catalyzed pathways reported below.

As touched upon in the introduction, locating relevant transition states fell beyond the scope of this study for the following two reasons: ruggedness of the energy landscape and the relatively large system size. In particular, the floppiness of Si−O−Si angles in the zeolite produced substantial framework relaxation along reaction pathways, making for a rugged energy landscape littered with many saddle points unrelated to the process of interest. To overcome this problem, we applied the nudged elastic band (NEB) method within the ONIOM formalism[16] for finding elusive transition states (results not shown). However, even this approach failed in the present application, because initial−guess pathways failed to capture the nature of zeolite relaxation. The failure of NEB thus necessitates a more exhaustive search for saddle points, which is computationally too expensive given the large quantum cluster size (~400 electrons). As such, we rely below on the nexus between experimental data and intermediate energetics to elucidate benzofuran production.

We used a finite cluster model for HZSM-5.[17,18] Fermann et al.[18] have shown that such finite zeolite clusters can provide an excellent alternative to more expensive periodic models for the calculation of reaction energies, because true long−range forces approximately cancel when computing energy differences between nearby configurations.[18] Following Agarwal et al.,[17] the HZSM-5 cluster is centered on O(13),[19] a catalytically important site because of its location at the intersection of the straight and zigzag channels where guest molecules can be accommodated.

HZSM-5 is modeled as an embedded cluster using the 2-layer ONIOM methodology[16] (see Figure 3). The quantum mechanical (QM) layer, which is treated at a high level of theory, is composed of 11 tetrahedral (T = Si or Al) sites, 30 oxygen atoms, and 1 acid site proton. The molecular mechanics (MM) layer, which is treated with a less expensive (and less accurate) level of theory, has 132 T sites and 311 O atoms. Zeolite clusters of this size have been demonstrated to converge relevant reaction energies with respect to system size.[18] For the high level of theory, we used density functional theory (DFT) with the B3LYP functional[20,21] and the 6-311G(d,p) basis set. This model chemistry has been shown to capture ~90% of barrier heights and reaction energies for acid−base chemistry in zeolites.[22] For the low level of theory, we used the universal force field (UFF),[23] which is generic and hence convenient but not optimized for any particular zeolite or composition. All atoms in the QM layer were allowed to relax freely, while the MM layer atoms were frozen at their crystallographically−determined positions, as in our previous work.[17] The QM layer is mechanically but not electronically embedded in the MM layer, that is, there are no external electrostatic interactions included in the quantum one−electron integrals. Dangling bonds on oxygen atoms at the periphery of the QM layer were capped with hydrogens. Computations were performed using Gaussian 09.[24] In what follows, we illustrate intermediate structures for reactions in zeolites using the format shown in Figure 3c, where only zeolite atoms within two bonds of the acid site are shown for visual simplicity. We reiterate that all calculations were performed using the cluster shown in Figure 3a and 3b.

Bonding in key structures was analyzed by computing atomic charges using the electrostatic potential (ESP) procedure of Kollman and co-workers.[25,26] This ensured that our calculations are reasonably well converged with respect to basis set by comparing with ESP charges from B3LYP/6-311G++(d,p), which contains more diffuse functions. The ESP charges also pointed to the most important Lewis structures along the reaction pathways, which assisted in interpreting DFT results in light of RING predictions.


dx.doi.org/10.1021/cs4003904 | ACS Catal. 2013, 3, 2012−2019

## 3. RESULTS AND DISCUSSION

**3.1. Experiments.** Figure 4 shows an Arrhenius plot of initial rates of benzofuran production from experiments using

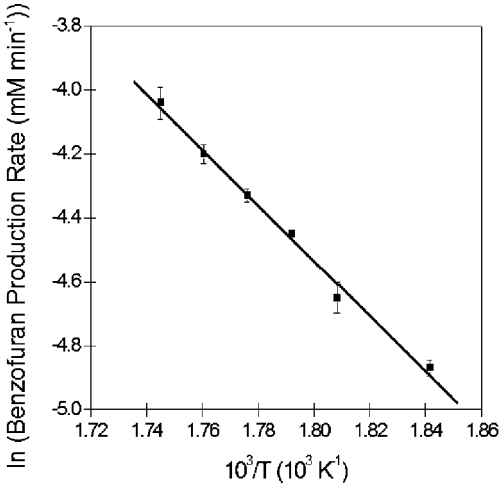


**Figure 4.** Arrhenius plot for the production of benzofuran from 1 M furan in heptane over 0.25 g of HZSM-5.

the methods described above. Additional plots containing the raw data are given in Figures S1 and S2 of the Supporting Information. The good linear fit in Figure 4 is consistent with a single, dominant mechanism in the temperature range 270−300 °C. The slope extracted from Figure 4 corresponds to an apparent activation energy of 72 ± 3 kJ/mol for the HZSM-5 catalyzed process. This apparent activation energy is inclusive of the following physical processes: diffusion, adsorption−desorption from the zeolite catalyst, and of course, chemical reaction. As such, this measured apparent activation energy is likely an upper bound for the activation energy of the rate-determining chemical reaction in benzofuran production.

**3.2. Calculations: Gas Phase Pathways.** *3.2.1. Ring-Opening Routes.* To establish energetic baselines for the zeolite-catalyzed processes of interest, we investigated the conversion of furan to benzofuran in the gas phase. RING[5] predicted that the acid-catalyzed conversion of furan to benzofuran proceeds by a sequence of protonation, ring-opening, ring-closing, and dehydration steps shown in Figure 2. The overall reaction involves two furan molecules condensing to give benzofuran and water. In our gas-phase calculations, we exhaustively mapped out intermediates for the first two steps in the process: the protonation and subsequent ring-opening of one furan molecule.Figure 5 shows the geometry-optimized structures and ground state electronic energies of the three protonated and five ring-opened species found in our gas-phase calculations. Energies are plotted relative to the ground state of furan. The zeolite solid acid is accounted for, approximately, by shifting the zero of energy by an amount equal to the energy required to strip a proton from the zeolite, assumed to be +1170 kJ/mol.[27] For example, a value of 300 kJ/mol in Figure 5 means that the gas-phase proton affinity of furan is 300 kJ/mol less than the assumed acidity of the zeolite, rendering protonation of furan endoergic by 300 kJ/mol. We emphasize that this is simply a shift in the zero of energy assumed in our gas-phase calculations, to facilitate comparison with the zeolite catalyzed systems. Figure 2 shows that protonation at C2 is consistent with three resonance structures, while protonation at

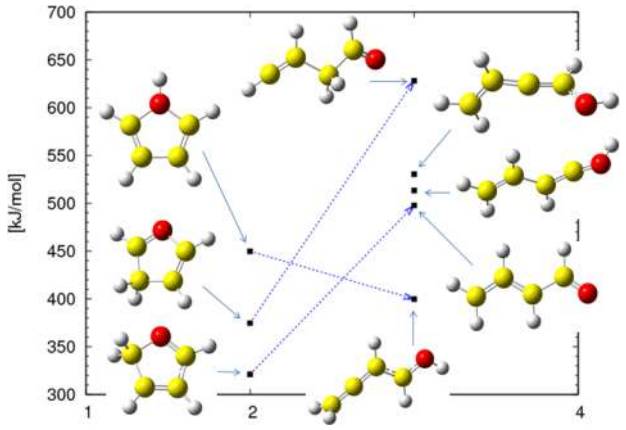


**Figure 5.** Gas-phase geometry-optimized structures and energies of all chemical species arising from the protonation and subsequent ring-opening of furan. These are the first two reactions in the ring-opening pathways from furan to benzofuran. Dotted blue arrows represent ring-opening reactions. Energies of all species are ground-state electronic energies plotted relative to furan, and include the energy cost of stripping a proton from the zeolite framework (+1170 kJ/mol).[27]

C3 only exhibits two resonance structures. This correlates with the fact that protonation at C2 is lower in energy than that at C3 by about 50 kJ/mol. ESP charges on the C2 protonated species (Figure S3 in Supporting Information) show that the dominant Lewis structure in the mechanism shown in Figure 2 is the one in which the positive charge is localized on the C5 atom (see Supporting Information for the rationale behind this assignment).

The dotted blue arrows in Figure 5 represent ring-opening reactions, and identify the structures that result from the ring-opening of each of the three protonated species. Two more ring-opened species can be generated by single hydrogen shifts, making a total of five protonated, ring-opened derivatives of furan that are stable in the gas phase. We note that the energetic order of protonated furan species does not correlate with the corresponding ring-opened structures, producing the line crossings in Figure 5.

The next step in the process is the alkylation of a second furan molecule at its C2 or C3 atom by one of the positively charged, ring-opened species. The open-ring species can react either at the carbon atom nearest, or the one farthest from the oxygen atom. Thus, each of the five ring-opened species can give rise to four alkylated derivatives, making a total of twenty alkylated species. Deprotonation, ring-closing, and dehydration steps complete the route to benzofuran. At each step of the process, many of the intermediates can interconvert via single hydrogen shifts, and are relatively closely spaced in energy. An interconnected web of pathways can thus be drawn from furan to benzofuran. Below, we map out two representative pathways with the lowest energy intermediates at the second (protonation) and third (ring-opening) steps.

Figure 6 shows the structures and energies of stable intermediates in a gas phase pathway originating with the protonation of furan at the C2 atom (step 2). This protonated furan ring opens (step 3) in a process that is endothermic by roughly 180 kJ/mol, to give the highest-energy intermediate in the pathway. In step 4, the open-ring species reacts at the carbon atom farthest from the oxygen, and alkylates a second furan molecule at the C2 position. Two branches of the pathway can be identified at the next step. The positively


dx.doi.org/10.1021/cs4003904 | ACS Catal. 2013, 3, 2012−2019

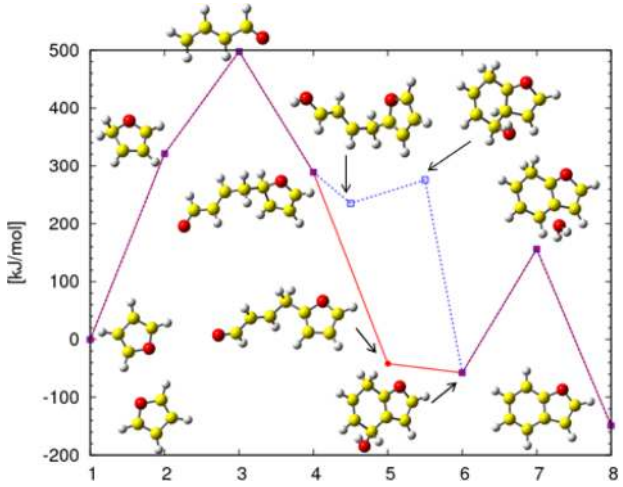


**Figure 6.** Gas-phase geometry optimized structures and energies of stable intermediates in a pathway arising from the protonation of furan at the C2 atom. Energies are plotted relative to the ground state electronic energy of two furans (step 1), and for positively charged species (i.e., those with positive energies), include the energy cost of stripping a proton from the zeolite framework (+1170 kJ/mol).[27]

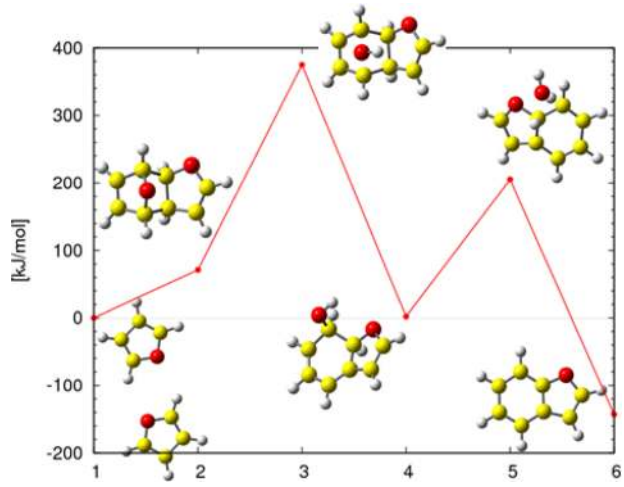


**Figure 7.** Stable intermediates and their energies in a gas phase pathway initiated by the Diels–Alder cycloaddition of two furan molecules. Energies are plotted relative to the ground state energy of two furans (step 1), and for positively charged species, include the energy cost of stripping a proton from the zeolite framework (+1170 kJ/mol).[27]

charged alkylated species can deprotonate and restore the aromaticity of the furan ring (Figure 6, solid red line, step 5) and then ring close (step 6). Alternatively, the alkylated species in step 4 can restore the aromaticity of the furan ring by a series of proton hops, and then ring close as a positively charged species (Figure 6, dotted blue line). Deprotonation restores the aromaticity of the furan ring at step 6, where the two branches of the pathway merge. Step 7 is a dehydration reaction, and a final deprotonation in step 8 leads to benzofuran.

A second representative pathway for the gas phase conversion of furan to benzofuran is shown in Figure S4 (Supporting Information) with energetics similar to those in Figure 6. This pathway starts with the highest energy intermediate at step 2, the furan derivative protonated at the O atom. The path to benzofuran is completed by ring-opening, alkylation, ring closing and dehydration steps, similar to the first pathway in Figure 6. In both pathways, dehydration is the penultimate step and occurs after the ring closing. Similar pathways can be constructed in which the dehydration step occurs before the ring closing (data not shown).

*3.2.2. Diels–Alder Routes.* A recent study of the conversion of furan to aromatic compounds over HZSM-5[3] postulated that the production of benzofuran occurs via a Diels–Alder condensation between two furans. Diels–Alder processes have also been invoked to explain the reactions between furanic compounds and olefins in the zeolite-catalyzed production of toluene and xylene.[14,28] To begin exploring this alternate route to benzofuran, we mapped out a representative Diels–Alder pathway in the gas phase in Figure 7. This pathway starts with a Diels–Alder cycloaddition reaction, in which one furan is the diene and the other is the dienophile. The cycloadduct can then be protonated at the bridge O atom, a reaction that is endothermic by roughly 300 kJ/mol. Deprotonation and dehydration steps complete this pathway to benzofuran, without any open ring intermediates. Similar pathways can be drawn in which a protonation step occurs before the cycloaddition.

In both classes of pathways, ring-opening and Diels–Alder, oxygen is removed through dehydration reactions. Hence, the occurrence of dehydration instead of decarbonylation reactions cannot be treated as a signature of a Diels–Alder process.[28] In the gas phase, the data in Figures 6, S4 (Supporting Information), and 7 suggest that the Diels–Alder route appears more likely because of intermediates 80–120 kJ/mol lower in energy than in the ring-opening pathways.

We show in the next section that this conclusion does not hold for the corresponding zeolite-catalyzed processes.

**3.3. Calculations: HZSM-5 Pathways.** With the gas-phase pathways as a guide, we explore the same processes in the HZSM-5 cluster, starting with the structural features. Figure 8 shows the geometry-optimized structures of stable intermediates in the zeolitic pathway following the ring-opening route. The two branches, I and II, correspond to the gas phase pathways of Figures 6 and S4 (Supporting Information)

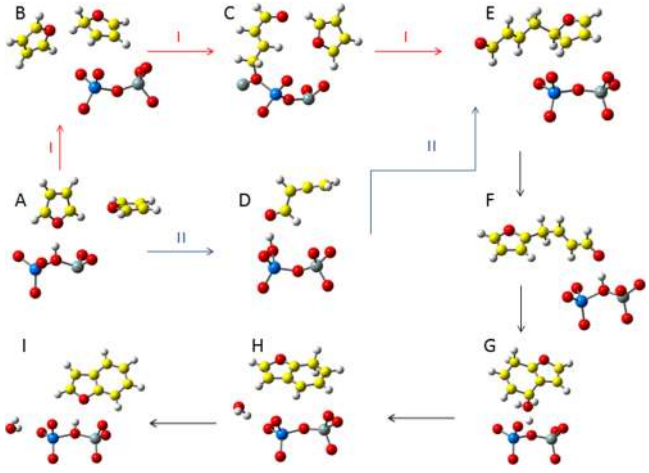


**Figure 8.** Geometry optimized structures of the stable intermediates in the zeolite-catalyzed, minimum energy pathway. In the zeolite, only the acid site and adjacent atoms are displayed, as in Figure 3c. Branch I is initiated by the stable protonation of furan at the C2 atom, while branch II proceeds by the transient protonation of furan at the O1 atom.


dx.doi.org/10.1021/cs4003904 | ACS Catal. 2013, 3, 2012–2019

respectively. The first step in the process is the adsorption of furan in the zeolite (Figure 8A). In the minimum energy configuration, one furan is hydrogen bonded to the zeolite acid site, at a distance of roughly 3.4 Å from the second furan molecule. Thus, there are two reacting furan molecules per acid site, consistent with the experimental observation that furan adsorbs in HZSM-5 at a furan-to-aluminum molar ratio of 1.73.[3]

In branch I, the zeolitic proton is transferred to the furan at the C2 position (Figure 8B), followed by the ring-opening of the protonated furan into an alkoxy species covalently bonded to the zeolite framework (Figure 8C). In branch II, the zeolitic proton is transferred to the O atom of the furan, but this protonated furan derivative is not a stable intermediate. It is instead a transition state on the proton hopping path between the central O atom of the zeolite cluster, and one of the other zeolite O atoms adjacent to the Al atom (Figure S5, Supporting Information). The transiently protonated furan ring opens to a species that is hydrogen bonded to the zeolite framework (Figure 8D). At the next step branches I and II merge, and the ring-opened species alkylate the second furan molecule (Figure 8E). Deprotonation (Figure 8F), ring-closing (Figure 8G), and dehydration (Figure 8H) steps lead to benzofuran (Figure 8I) with the loss of a water molecule.

We note that this mechanism is also a potential source of the larger polycyclic compounds, that is, coke, that can clog the pores of the zeolite and deactivate it. Similar to the ring-opening of the protonated furan discussed above, the positively charged, alkylated furan derivative (Figure 8E) can ring open and alkylate a third furan molecule. This process will result in species that are too big to diffuse out of the pores of HZSM-5, leading to the accumulation of carbon deposits and subsequent deactivation of the catalyst.

We next consider the Diels–Alder route to benzofuran inside the zeolite cavity. Figure 9 shows the geometry optimized

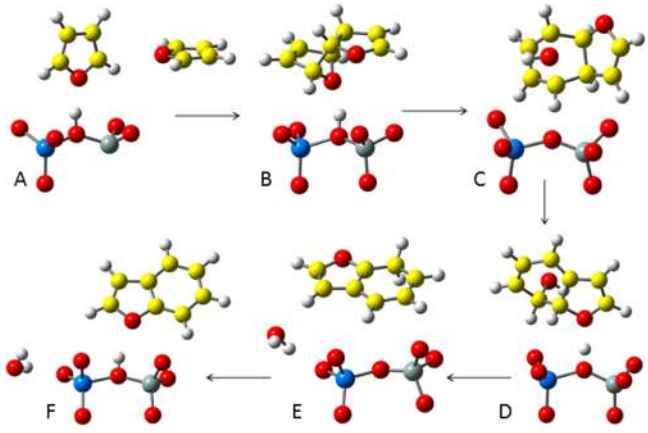


**Figure 9.** Geometry-optimized structures of the stable intermediates in the zeolite-catalyzed, Diels–Alder pathway.

structures of the stable intermediates along the pathway corresponding to the gas phase pathway in Figure 7. As with the indirect process discussed above, the first step in the direct route is the adsorption of two furans per zeolite acid site (Figure 9A). In the next step, the two furans undergo a Diels–Alder cycloaddition. In its lowest energy configuration, the cycloadduct is hydrogen bonded to the acid site at the furanic O atom (Figure S6, Supporting Information). However, the adduct cannot be stably protonated at the furanic O atom and is, therefore, an off-pathway dead end. In the lowest energy, on-pathway configuration (Figure 9B), the cycloadduct is hydrogen bonded to the acid site at the bridge O atom. Subsequently, the adduct is protonated at the bridge O atom (Figure 9C), following which, deprotonation (Figure 9D) and dehydration (Figure 9E) reactions lead to benzofuran (Figure 9F) with the loss of a water molecule.

We next consider the energetics of the ring-opening and Diels–Alder zeolite-catalyzed processes in HZSM-5. The solid red and dotted blue lines in Figure 10 show the energies of the

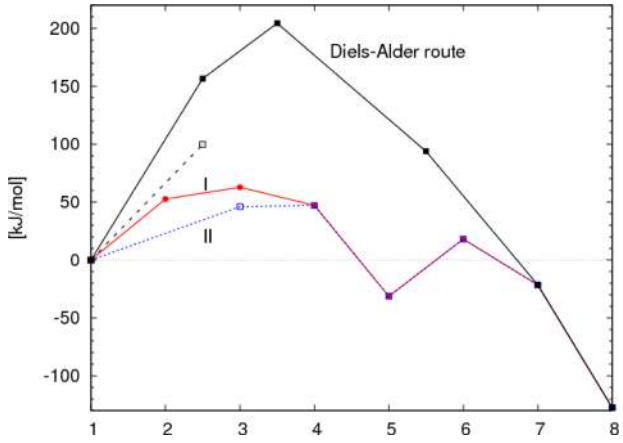


**Figure 10.** Energies of the intermediates in Figure 8 are shown in the solid red (branch I) and dotted blue (branch II) lines. Comparison with Figures 6 and S4 (Supporting Information) shows that the HZSM-5 catalyst energetically stabilizes the intermediates leading to benzofuran. The solid black line shows the energies of intermediates in the zeolite-catalyzed Diels–Alder route (Figure 9). The dashed black line leads to the lowest energy configuration of the cycloadduct in the zeolite.

intermediates in branches I and II of the indirect route respectively. The corresponding structures are shown in Figure 8. Comparison with Figures 6 and S4 (Supporting Information) shows that the zeolite greatly stabilizes the intermediates on the pathway leading to benzofuran with active intermediate energies reduced from about 500 kJ/mol to roughly 50 kJ/mol, a reduction of 90%. This intermediate energy of 50 kJ/mol fits nicely into the "energy budget" determined by our experimentally determined apparent activation energy of 72 ± 3 kJ/mol.

The substantial stabilization of the intermediates seen in the zeolite, relative to the gas phase, deserves further comment. In the gas-phase pathways, the proton donor (HZSM-5) and the proton acceptor (furan) are assumed to be infinitely far from each other to remove the catalytic effect while still having a zero of energy that is common between gas-phase and zeolite-catalyzed energy diagrams. In contrast, in the computed zeolite-catalyzed pathways, the proton motion is over a distance of only a few ångstroms. The approximately 500 kJ/mol gas-phase energy scale thus reflects the difference in proton affinity (PA) between the zeolite (with a relatively large PA) and furan (with a relatively small PA). When the protonated furan is explicitly inserted into the deprotonated zeolite in the zeolite-catalyzed system, strong electrostatic attractions (responsible for the large zeolite PA) become re-established, which serve to substantially stabilize the system.

While the ring-opening and Diels–Alder pathways are energetically similar in the gas phase, the situation for the


dx.doi.org/10.1021/cs4003904 | ACS Catal. 2013, 3, 2012–2019

reaction inside the zeolite is quite different. The solid black line in Figure 10 shows the energies along the zeolite-catalyzed Diels–Alder route. These intermediates are also stabilized relative to the corresponding gas-phase structures, but are much higher in energy than the ring-opening zeolite-catalyzed pathway.

The geometries of the cycloadduct along the Diels–Alder pathway (Figure 10, solid black line), and in the off-pathway dead end configuration (Figure 10, dashed black line), offer a clue to the high energies along the Diels–Alder route in the zeolite. The hydrogen bond distance between the cycloadduct O atom and the central O atom of the zeolite cluster is the same (2.6 Å) in both configurations. However, the configuration along the Diels–Alder pathway is a "tighter fit" inside the pore, with three other atoms of the guest molecule located less than 2.9 Å from a zeolite framework atom; the corresponding distance for the dead end configuration is 3.4 Å. By comparison, atomic van der Waals diameters are typically in the range 3–4 Å.

These computational results, taken together with the experiments reported herein, provide strong evidence that the HZSM-5 catalyzed conversion of furan to benzofuran proceeds by a ring-opening pathway involving open ring intermediates, rather than the Diels–Alder route. The stable intermediates along the Diels–Alder pathway are seen to be higher in energy than the experimentally measured apparent activation energy. Hence, we can rule out the Diels–Alder route to benzofuran in HZSM-5, even without locating transition states along any of the pathways.

While this analysis applies to the formation of benzofuran from furan in HZSM-5, it is important to note that these results do not necessarily apply to other potential Diels–Alder reactions such as furan condensation with olefins. Specific reaction mechanisms depend on the reactant species, catalyst type, and reactant, intermediate, and product energetics. The results of this study serve to highlight the importance of examining individual key steps in biomass conversion to determine which mechanisms are favorable for a given system.

## 4. SUMMARY AND CONCLUSIONS

We have performed kinetics experiments and quantum calculations on embedded clusters to investigate the conversion of furan to benzofuran in the zeolite catalyst HZSM-5, a key step in the catalytic fast pyrolysis of biomass to biofuels. The reaction was probed experimentally by placing the zeolite in contact with solution-phase furan in heptane and detecting benzofuran over the temperature range 270–300 °C, which yielded an apparent activation energy of 72 ± 3 kJ/mol. The reaction was modeled in gas and zeolite phases by computing energies for the following two pathways: a Diels–Alder mechanism assumed in interpretations of experimental data, and a ring-opening pathway predicted by the software RING.

Quantum calculations for this reaction were performed using the ONIOM embedded cluster approach. We computed energies for reactants, products, and all intermediate steps; locating transition states was not possible because of system size and the ruggedness of the potential energy. The gas-phase Diels–Alder pathway was found to pass through a high-energy intermediate roughly 380 kJ/mol above the reactant energy; this reduced to about 200 kJ/mol in HZSM-5. In contrast, the gas-phase ring-opening mechanism passes through an intermediate roughly 500 kJ/mol above the reactant energy; this reduced by 90% in the zeolite to about 50 kJ/mol, which agrees reasonably well with the experimentally determined activation energy of 72 kJ/mol.

These experimental and computational results suggest the importance of the ring-opening mechanism for this key step in making biofuels. However, recent results[14,29] suggest that Brønsted acidity is relatively ineffective at catalyzing Diels–Alder cycloaddition, while Lewis acidity is much more effective at catalyzing such chemistry. In future work, we will apply the computational methods described above to investigate whether Lewis acidity may facilitate benzofuran production through Diels–Alder pathways in HZSM-5 and other zeolites. We will also pursue direct transition state calculations to provide complete microkinetic pathways for these important processes in biofuel production.

## ■ ASSOCIATED CONTENT

### Supporting Information

Structures, energies, and atomic charges of key species in benzofuran formation. This information is available free of charge via the Internet at http://pubs.acs.org/.

## ■ AUTHOR INFORMATION

### Corresponding Author

*E-mail: auerbach@chem.umass.edu.

### Notes

The authors declare no competing financial interest.

## ■ ACKNOWLEDGMENTS

We acknowledge generous funding from NSF (CBET-0932777 and EFRI-0937895) and from the Catalysis Center for Energy Innovation, an Energy Frontier Research Center funded by the U.S. Department of Energy, Office of Science, Office of Basic Energy Sciences under award number DE-000SC0001004. We greatly appreciate Srinivas Rangarajan's extensive help with the program RING and Figure 2. We also thank an unknown reviewer for pointing out that the ring-opening mechanism can potentially lead to coke.

## ■ REFERENCES

(1) Auerbach, S. M., Carrado, K. A., Dutta, P. K., Eds. *Handbook of Zeolite Science and Technology*; Marcel Dekker, Inc.: New York, 2003.
(2) Vispute, T. P.; Zhang, H.; Sanna, A.; Xiao, R.; Huber, G. W. *Science* **2010**, *330*, 1222–1227.
(3) Cheng, Y.-T.; Huber, G. W. *ACS Catal.* **2011**, *1*, 611–628.
(4) Cheng, Y.-T.; Jae, J.; Shi, J.; Fan, W.; Huber, G. W. *Angew. Chem., Int. Ed.* **2012**, *51*, 1387–1390.
(5) Rangarajan, S.; Bhan, A.; Daoutidis, P. *Ind. Eng. Chem. Res.* **2010**, *49*, 10459–10470.
(6) Vasiliu, M.; Guynn, K.; Dixon, D. A. *J. Phys. Chem. C* **2011**, *115*, 15686–15702.
(7) Assary, R. S.; Redfern, P. C.; Hammond, J. R.; Greeley, J.; Curtiss, L. A. *J. Phys. Chem. B* **2010**, *114*, 9002–9009.
(8) Assary, R. S.; Redfern, P. C.; Hammond, J. R.; Greeley, J.; Curtiss, L. A. *Chem. Phys. Lett.* **2010**, *497*, 123–128.
(9) Assary, R. S.; Redfern, P. C.; Greeley, J.; Curtiss, L. A. *J. Phys. Chem. B* **2011**, *115*, 4341–4349.
(10) Assary, R. S.; Curtiss, L. A. *Energy Fuels* **2012**, *26*, 1344–1352.
(11) Qian, X. *J. Phys. Chem. A* **2011**, *115*, 11740–11748.
(12) Qian, X. *Top. Catal.* **2012**, *55*, 218–226.
(13) Cheng, L.; Curtiss, L. A.; Assary, R. S.; Greeley, J.; Kerber, T.; Sauer, J. *J. Phys. Chem. C* **2011**, *115*, 21785–21790.
(14) Williams, C. L.; Chang, C.-C.; Do, P.; Nikbin, N.; Caratzoulas, S.; Vlachos, D. G.; Lobo, R. F.; Fan, W.; Dauenhauer, P. J. *ACS Catal.* **2012**, *2*, 935–939.
(15) Rangarajan, S.; Bhan, A. Private communication.

(16) Vreven, T.; Morokuma, K. *Annu. Rep. Comput. Chem.* **2006**, *2*, 35−51.
(17) Agarwal, V.; Huber, G. CW.; W., C. C., Jr.; Auerbach, S. M. *J. Catal.* **2010**, *269*, 53−63.
(18) Fermann, J. T.; Moniz, T.; Kiowski, O.; McIntire, T. J.; Auerbach, S. M.; Vreven, T.; Frisch, M. J. *J. Chem. Theory Comput.* **2005**, *1*, 1232−1239.
(19) Olson, D. H.; Kokotailo, G. T.; Lawton, S. L.; Meier, W. M. *J. Phys. Chem.* **1985**, *85*, 2238−2243.
(20) Becke, A. D. *J. Chem. Phys.* **1993**, *98*, 5648−5652.
(21) Stephens, P. J.; Devlin, F. J.; Chabalowski, C. F.; Frisch, M. J. *J. Phys. Chem.* **1994**, *98*, 11623−11627.
(22) Fermann, J. T.; Blanco, C.; Auerbach, S. *J. Chem. Phys.* **2000**, *112*, 6779−6786.
(23) Rappe, A. K.; Casewit, C. J.; Colwell, K. S.; Goddard, W. A.; Skiff, W. M. *J. Am. Chem. Soc.* **1992**, *114*, 10024−10035.
(24) Frisch, M. J.; Trucks, G. W.; Schlegel, H. B.; Scuseria, G. E.; Robb, M. A.; Cheeseman, J. R.; Scalmani, G.; Barone, V.; Mennucci, B.; Petersson, G. A.; Nakatsuji, H.; Caricato, M.; Li, X.; Hratchian, H. P.; Izmaylov, A. F.; Bloino, J.; Zheng, G.; Sonnenberg, J. L.; Hada, M.; Ehara, M.; Toyota, K.; Fukuda, R.; Hasegawa, J.; Ishida, M.; Nakajima, T.; Honda, Y.; Kitao, O.; Nakai, H.; Vreven, T.; Montgomery, J. A., Jr.; Peralta, J. E.; Ogliaro, F.; Bearpark, M.; Heyd, J. J.; Brothers, E.; Kudin, K. N.; Staroverov, V. N.; Kobayashi, R.; Normand, J.; Raghavachari, K.; Rendell, A.; Burant, J. C.; Iyengar, S. S.; Tomasi, J.; Cossi, M.; Rega, N.; Millam, J. M.; Klene, M.; Knox, J. E.; Cross, J. B.; Bakken, V.; Adamo, C.; Jaramillo, J.; Gomperts, R.; Stratmann, R. E.; Yazyev, O.; Austin, A. J.; Cammi, R.; Pomelli, C.; Ochterski, J. W.; Martin, R. L.; Morokuma, K.; Zakrzewski, V. G.; Voth, G. A.; Salvador, P.; Dannenberg, J. J.; Dapprich, S.; Daniels, A. D.; Farkas, O.; Foresman, J. B.; Ortiz, J. V.; Cioslowski, J.; Fox, D. J. *Gaussian 09*, revision B.01; Gaussian, Inc.: Wallingford, CT, 2009.
(25) Singh, U. C.; Kollman, P. A. *J. Comput. Chem.* **1984**, *5*, 129−145.
(26) Besler, B. H.; K., M. M., Jr.; Kollman, P. A. *J. Comput. Chem.* **1990**, *11*, 431−439.
(27) Haw, J. F. *Phys. Chem. Chem. Phys.* **2002**, *4*, 5431−5441.
(28) Cheng, Y.−T.; Huber, G. W. *Green Chem.* **2012**, *14*, 3114−3125.
(29) Nikbin, N.; Do, P. T.; Caratzoulas, S.; Lobo, R. F.; Dauenhauer, P. J.; Vlachos, D. G. *J. Catal.* **2013**, *297*, 35−43.